Arch. Metall. Mater. **68** (2023), 1, 331-338

DOI: https://doi.org/10.24425/amm.2023.141509

A. BAGHERI[1], A. BOOCHANI[2*], S.R. MASHARIAN[1], F.H. JAFARPOUR[3]

THERMODYNAMIC PHASE DIAGRAM AND PHONON STABILITY, ELECTRONIC AND OPTICAL PROPERTIES OF FeVSb: A DFT STUDY

Mechanical, electronic, thermodynamic phase diagram and optical properties of the FeVSb half-Heusler have been studied based on the density functional theory (DFT) framework. Studies have shown that this structure in the MgAgAs-type phase has static and dynamic mechanical stability with high thermodynamic phase consistency. Electronic calculations showed that this compound is a p-type semiconductor with an indirect energy gap of 0.39 eV. This compound's optical response occurs in the infrared, visible regions, and at higher energies its dielectric sign is negative. The Plasmon oscillations have occurred in 20 eV, and its refraction index shifts to zero in 18 eV.

Keywords: DFT; Thermodynamic Phase Diagram; Phonon; Electronic Properties; Optical Properties

1. Introduction

In recent years, the half-Heusler family of Fe-based compounds, such as FeMSb(M = V,Nb), has received much attention from researchers [1-4]. Half-Heusler structures with XYZ stoichiometry that X, Y are transition metals and Z belong to II-V periodic table, exhibit different and interesting physical behaviors such as excellent thermoelectric properties [5,6], polar magneto-optic Kerr effect at room temperature [7], superconductivity [8], topology properties [9,10], and magneto resistance and magneto caloric effect [11,12]. Fe-based half-Heusler compounds, such as FeVSb with 18 valence electrons, have excellent thermoelectric performance in the pure case and presence of impurities [13-15]. Yang et al., showed that FeVSb compound has a high power factor and a narrow energy gap of 0.32 eV [16]. Young et al., predicted the thermoelectric behavior of this compound and showed that FeVSb is an n-type semiconductor with high electrical resistance of about 0.2 mW to 20 mW [17] at room temperature with Seebeck amount of –70 μVK^{-1} in 300K. Chemical substitution is used as a definitive solution to increase the thermoelectric performance of materials. In recent years, many reports of various impurities have been replaced to improve the thermoelectric quality of FeVSb compound. Stadnyk et al., showed that Cu's replacement with Fe1-xCuxVSb leads to the displacement of the Fermi surface to its conductor and the occurrence of semi-metallic behavior with increasing electron conductivity [18].

Hasan et al reported that the combination of FeVSb polluted with Se atoms retains n-type conductivity in this material and leads to a significant reduction in network thermal conductivity [14]. Other reports have suggested the Zr, Ti, and Co impurities in this structure. Meanwhile, Sb impurity has significantly increased the Merit coefficient by 0.31 at 573K in the $FeV_{1.15}Sb$ case [2,4]. Hf's replacement in FeVSb has been one of the successful reports of a reduction in lattice thermal conductivity due to an increase in the scattering of lattice faults due to the presence of this impurity [19-23]. Another successful way to improve thermoelectric performance is to create a thin film or nanostructured film. In this regard, Liu et al examined the thin-film FeVSb film diluted with the Ti atom and found that amorphous $(FeVSb)_{1-x}Ti_x$ films had much higher power factor and merit coefficient values than pure FeVSb. In this work, we decided to examine the structural features and electronic and optical behavior of the widely used FeVSb compound. The following topics are summarized in this article: In the first part, the structural stability of FeVSb from the mechanical, dynamic and thermodynamic perspectives is calculated by calculating the elastic coefficients, phonon distribution curve to show the mechanical resistance and demonstrate the heat capacity of this structure at the gamma point symmetry in the Brillouin zone, and also the phase diagram stability diagram

[1] DEPARTMENT OF PHYSICS, HAMEDAN BRANCH, ISLAMIC AZAD UNIVERSITY, HAMEDAN, IRAN
[2] DEPARTMENT OF PHYSICS, KERMANSHAH BRANCH, ISLAMIC AZAD UNIVERSITY, KERMANSHAH, IRAN
[3] PHYSICS DEPARTMENT, BU-ALI SINA UNIVERSITY, 65174-4161 HAMEDAN, IRAN

* Corresponding Author: arash_bch@yahoo.com

with a waste accessible region. In the second part, electronic behavior includes the band structure and density of state. In its optical behavior section, including dielectric, energy loss functions, absorption, and refraction coefficients were presented in calculating the basic principles of DFT to indicating its application in the electronic and optoelectronic industry.

2. Computational Methods

Electronic and optical specifications of the FeVSb compound, as well as its mechanical and elastic stability, were calculated using the full potential of the linear augmented plane wave (FP-LAPW) method within the Wien2K code by generalized gradient approximation (GGA) [24,25]. Optimized values of software input parameters such as separation energy, KPoint, RKmax and lmax are selected as –8.0Ryd, 4000, 8.5, and 10, respectively. Also, optimized parameters in the Quantum Espresso calculations such as ECut, KPoint and force convergence selected to 150, 15*15*15, and 10^{-6}, respectively. The FeVSb compound has a MgAgAs-type structure by $F\bar{4}3m$ space groups with 4a (0, 0, 0), 4b (1/2, 1/2, 1/2) and 4c (1/4, 1/4, **1/4)** for Sb, V and Fe atoms, respectively (Fig. 1). To show the mechanical stability of the FeVSb combination, the energy-volume curves to show the equilibrium volume and elastic constants at zero Kelvin are calculated which we ignore by applying small approximations to the lattice vibrations. Next, to show the thermodynamic stability, we use the phase diagram, the variable of which is the chemical potential. We will also examine phonon lattice vibrations. In Quantum Espresso software, by selecting the smearing and degauss switches to 0.2, which provide Fermi energy expansion, we look at the phonon band structure diagram at temperatures above zero and room temperature.

3. Results

3.1. Structural properties

The energy-volume (E-V) diagram of the unit cell contains crucial points about the crystalline structure of matter such as lattice constant, bulk modulus, the derivative of bulk modulus, and equilibrium volume, the ground state point. The changes in energy relative to the volume and fit with the Brich-Mornaghan equation [27] (Eq. (1)) has a positive concavity and a (minimum) equilibrium point for the stable material in the mechanical view, which indicates the minimum crystal energy at this point.

$$E(V) = E_0 + \frac{BV}{B'}\left[\frac{1}{B'-1}\left(\frac{V_0}{V}\right)^{B'} + 1\right] \quad (1)$$

In the FeVSb compound, we changed its volume unit cell from -20% to 20% with 5% steps in Fig. 1 for the ferromagnetic (FM), and non-magnetic (NM) phases are entirely on top of each other. It is shown that the E-V diagram in Fig. 1 has a minimum point in the symmetry form, which refers to its good stability with high hardness. The E-V curve results, including equilibrium volume, lattice constant, bulk modulus, derivative, and total crystal energy, are listed in TABLE 1. The total magnetic moment of the FeVSb follows from the slider-Pauling rule, and the magnetic moment has been reduced to zero.

TABLE 1

The lattice parameter (a), bulk modulus (B) *and its pressure derivative* (B'), and formation energies in Ferromagnetic and Non-magnetic phases (E_f) for ScPtBi compound

FeVSb	*a* (°A)	*B* (GPa)	*B'* (GPa)	E_f (eV)	*Eg* (eV)
NM	5.785	169.81	4.38	–0.332	0.39
FM	5.714	169.82	4.38	–0.331	
Other works					
NM[a]					0.34
NM[b]	5.826				0.46

a. [28], b. [2] via LDA.

To further investigate the mechanical stability of the FeVSb compound, the elastic constants and related parameters such as Yong modulus, Shear modulus, melting point, poison's ratio (v), and the bulk to shear modulus ratio have been calculated in TABLE 2. To study the mechanical properties crystal, the mechanical response of the crystal (stress) to different strains must be studied. Due to the cubic structure of the FeVSb case, three elastic constants of C_{11}, C_{12} and C_{44} can be defined for it. Consid-

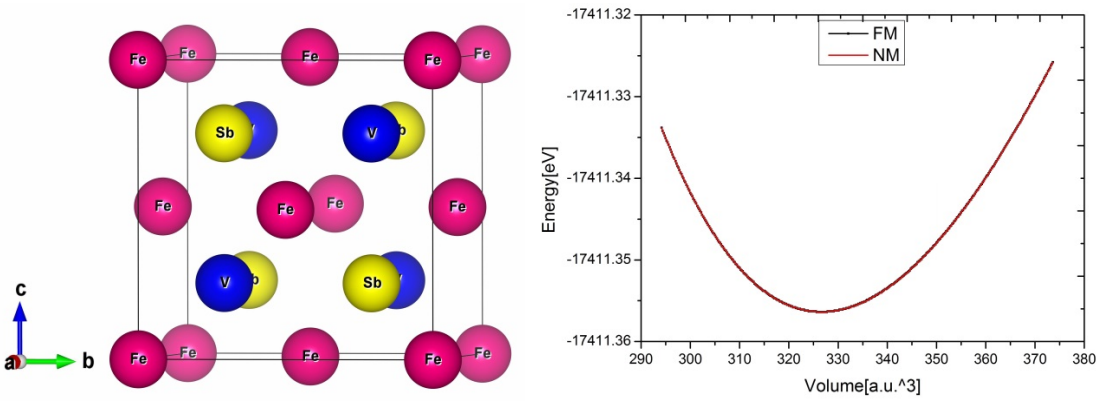

Fig. 1. (left) The crystal structure (right) The E-V diagram in two FM and NM mode of the FeVSb

ering the high values of this parameters and conditions of the (2) equation, it can be said that the FeVSb has elastic stability [29].

$$C_{11} > 0,\ C_{11} - C_{12} > 0 \text{ and } C_{44} > 0 \quad (2)$$

Another significant coefficient of elasticity is the elastic anisotropy (A) coefficient (Eq. (3)), one for the completely homogeneous structure. Based on equation (3), the FeVSb elastic anisotropy is equivalent to 1.69, which refers to the isotropic elastic response.

$$A = \frac{2C_{44}}{(C_{11} - C_{12})} \quad (3)$$

Another parameter calculated in this section is the shear modulus (G) which is equal to the ratio of shear stress to shear strain and is calculated according to Equation (3) with elastic coefficients. The elasticity indicates how much the material tolerates the forces that cause it to deform, how much it resists it, and to what extent it undergoes change. The material deforms if it is compressed or stretched along an axis. Yang's modulus is equal to the stress-strain ratio. This parameter indicates the body's resistance to longitudinal deformation in a particular direction when a force in the opposite direction enters the crystal. The value obtained for this module in TABLE 2, it can be concluded that FeVSb is classified as a hard material. The Poisson (v) coefficient is equal to the ratio of transverse strain to longitudinal strain and indicates the degree of crystal stability against shear deformation. The maximum value of this coefficient is about 0.5, and it is related to rubber, which is very resistant to compression. According to TABLE 2, the numerical value of v is about 0.13, which indicates the high elasticity of this material and its low tendency to be plastic. Melting temperature is a sufficient quantity in the application of materials obtained from Equation (6), and it was observed that FeVSb is one of the materials with a high melting temperature.

$$G_V = (C_{11} - C_{12} + 3C_{44})/5 \quad (3)$$

$$E = \frac{9BG}{(3B+G)} \quad (4)$$

$$\upsilon = \frac{3B-2G}{2(3B+G)} \quad (5)$$

$$T_m = \left[553\text{K} + \left(9.91\frac{\text{K}}{\text{GPa}}\right)C_{11}\right] \quad (6)$$

3.1.2. Thermodynamic Phase Diagram

The thermodynamic phase diagram stability diagrams of the FeVSb compound are shown in Fig. 2. In both charts, all possible probabilities for forming of crystals, including Fe, V, and Sb atoms, were considered to investigate the stability of their MgAgAs-type structure. The Gibbs free energy structure of the Heusler FeVSb semiconductor can be calculated according to the subunit relationship according to the atomic chemical potentials (m).

$$\mu_{Fe} + \mu_V + \mu_{Sb} = g^{bulk}_{FeVSb} \quad (7)$$

For every three atoms in the phase diagram, there will be accessible areas. We consider the potential chemical changes

TABLE 2

Calculated values of elastic constants (C_{11}, C_{12}, C_{44}) (in GPa), shear modulus (G) (in GPa), (B/G) ratio, Young's modulus (E) (in GPa), Poisson ratios (v), melting tempreture (T_m ±300 in K), and percentage of anisotropy (A) for FeVSb with GGA

Compound	C_{11}	C_{12}	C_{44}	E	G	υ	B/G	A	T_m ±300
FeVSb	332.68	187.97	244.71	520.25	175.76	0.132	0.966	1.69	2519.1
Other works									
FeVSb[a]	307	102	54	184	70	0.319			

a. Ref. [3]: theoretical values via CASTEP code.

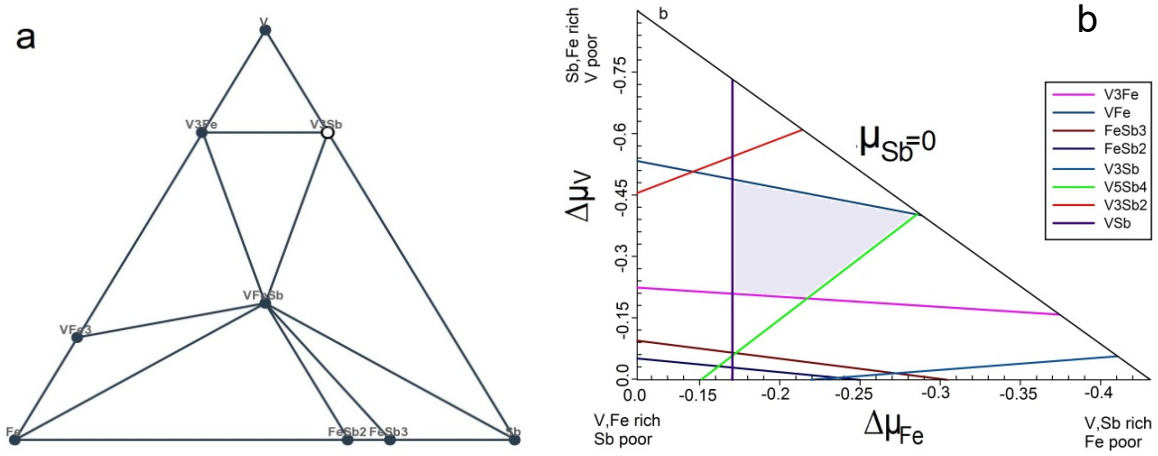

Fig. 2. (a) The ternary phase diagram, (b) The thermodynamic phase diagram stability of FeVSb as the chemical potentials changing

of atoms ($\Delta\mu_i$) between the minimum and maximum values. The *i* index represents the number of *i* atom. Thus the minimum value of m_i is where the *i* atom leaves the FeVSb bulk structure, and the maximum value is obtained when this atom is crystallized in its bulk structure. Changes are obtained from the following relationships [34-36]:

$$G_{\mathrm{FeVSb}} - g_{\mathrm{VSb}} \le \Delta\mu_{\mathrm{Fe}} \le g_{\mathrm{Fe}}^{bulk} \quad (8)$$

$$G_{\mathrm{FeVSb}} - g_{\mathrm{FeSb}} \le \Delta\mu_{\mathrm{V}} \le g_{\mathrm{V}}^{bulk} \quad (9)$$

$$G_{\mathrm{FeVSb}} - g_{\mathrm{VFe}} \le \Delta\mu_{\mathrm{Sb}} \le g_{\mathrm{Sb}}^{bulk} \quad (10)$$

In the above relationships, g^{bulk} denotes the maximum value of μ_i. In Fig. 2(a), the ternary phase diagram is seen, in each corner the chemical potential of Fe, V, and Sb atoms exist. All possible structures between these three atoms are shown with dots on the figure. The connection of all these points has resulted in the possibility of FeVSb crystallization in the semiconductor phase. Fig. 2(b) shows the probability of stability of this structure based on changes in Fe and V atoms' chemical potential as a hatched area. Therefore, as can be seen, FeVSb will be thermodynamically stable in the MgAgAs-type semiconductor phase.

3.1.3. The Phonon Dispersion

The phonon bandstructure curves along with the high symmetry directions in the first region of Brillouin zone, and its density of states (DOS) of the FeVSb compound are shown in Fig. 3. As it turns out, all phonon modes have a positive frequency, and there is no negative phonon branches. Therefore, we conclude that the FeVSb semiconductor composition in the MgAgAs-type cube structure is dynamically stable. Nine vibrational modes of this shape are due to the three atoms in the unit cell, which three are the lower modes between zero to 175 cm^{-1}, are acoustic branches, and six others (200 cm^{-1} to 360 cm^{-1}) are the optical branches. The narrow frequency gap between these two frequency regions with a value of about 20 cm^{-1} is due to the difference in the atoms in this compound's unit cell. Also, from the DOS curve (Fig. 3(b)), it is observed that in the low-frequency region, the highest phonon distribution is related to Sb atom, which is due to the high atomic mass of this element compared to the other two atoms in FeVSb structure. At higher frequencies, the optical modes, the lighter Fe and V atoms play a dominant role in the phonon distribution.

3.2. Electronic Properties

To investigate the electronic properties, we studied the electronic bandstructure and density of states of FeVSb compounds. By examining the DOS diagrams, the share of different atomic orbitals can be determined. The below area of the DOS curve in each energy interval is equal to the number of allowed electron states. Calculations performed with non-spin GGA approximation. According to Fig. 4, the non-magnetic p-type semiconductor behavior with a 0.39 eV gap is observed, which agrees with others [2,28]. The bandstructure diagram shows that the valence band maximum is at point L and the minimum of its conduction band is at X point. It was observed that in these two points, the slope of the electron levels curve is more than other directions, and besides, with the increase of energy level, the slope of the curves in 1.5 eV energy onwards has increased sharply. On the other hand, in the lower energies of valence, curves' slope has increased, so this compound has very high mobility for electrons and holes in exciting conditions. In the higher energies of the conduction band, the effective mass of the electron is greatly reduced. It is also clear that in both the conduction and valence bands, the significant share of electronic states is related to Fe and V atoms.

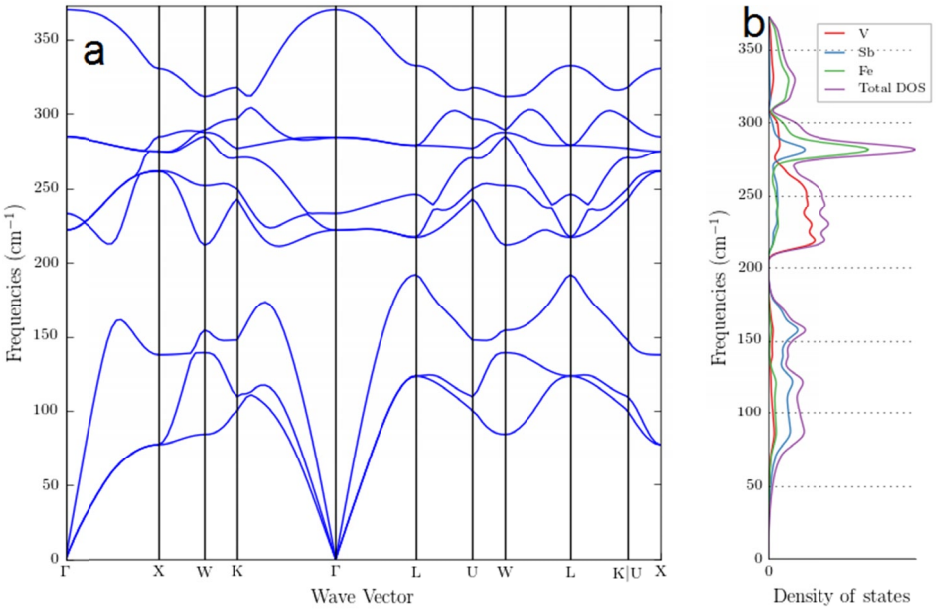

Fig. 3. (a) Phonon bandstructure and, (b) The DOS of FeVSb

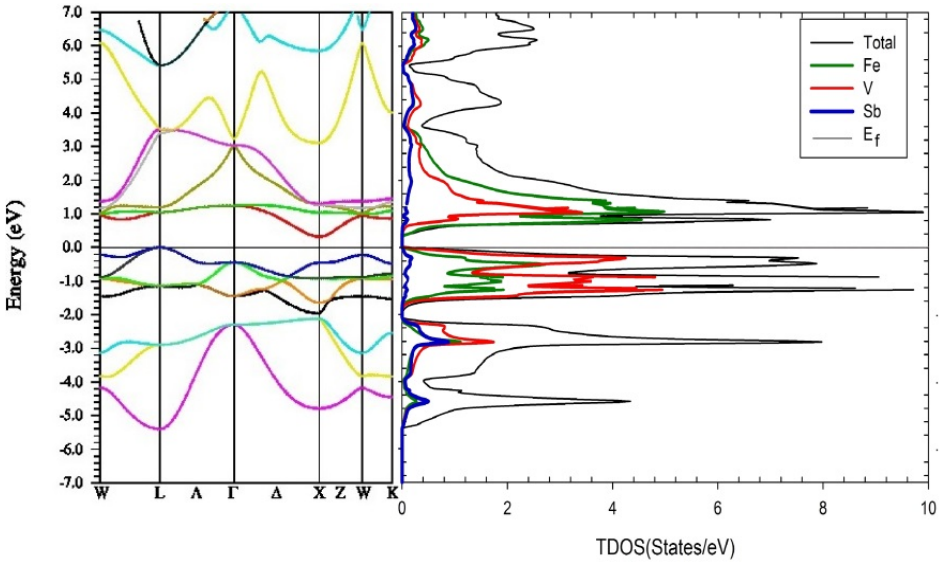

Fig. 4. The bandstructure and DOS of the FeVSb compound

3.3. Optical Properties

This section has examined optical parameters such as real and imaginary parts of the dielectric function, electron energy loss function, refractive index, and optical absorption coefficients. For optical calculations, we used the 20000 KPoints and the random phase approximation (RPA). The dielectric function ($\varepsilon(\omega)$) of the optical spectrum is very useful in determining the overall crystal band structure. The dielectric function is not directly derived from optical measurements. Functions that are directly obtained include: Reflection coefficient (R), refractive index ($n(\omega)$) and extinction coefficient ($K(\omega)$). As can be seen in Equation (7), the dielectric function is a mixed-function consisting of two real parts and an imaginary part that can be connected by the Kramers-Kronig relations relationship.

$$\varepsilon(\omega) = \varepsilon_1(\omega) + i\varepsilon_2(\varepsilon) \tag{7}$$

In Fig. 5(a) , it can be seen that the $\varepsilon_1(\omega)$ is increased as the photon energy and we see a long sharp peak in the infrared region and then decreased in the visible edge and show the semiconducting behavior. The first root of this function is at the ultraviolet edge and the second root is in the range of 7.3 eV energy and is a negative sign up to 20 eV, and again in this energy the sign is positive and we see another root. From 20 eV onwards, the response to light has been virtually zero. Areas with a negative sign of the dielectric function refer to semi-material or metallic behaviors. The peaks in the imaginary part of the dielectric function ($\varepsilon_2(\omega)$) correspond to the DOS diagram's critical points and show the inter- and intra-band optical transitions.

Fig. 5(b) shows the imaginary part of the FeVSb dielectric function. At low energies, we see a gap in it that is entirely in agreement with its DOS curve. In the infrared region, we see a sharp Dirac peak that representing the transfer of electrons from full to empty levels in this energy. Still this condition is not very stable and the decreasing process begins quickly, and from the visible edge onwards, it has been reduced with a lower slope. In this area and up to the 10 eV range, we still see optical transitions, and after this energy, we will have no transitions and, as a result, light absorption. In energies where the real part of the dielectric function is zero, the imaginary part is also reduced with a steep slope. Electron energy-loss function (ELoss) is one of the most important quantities to determine the macroscopic and microscopic properties of solids, proportional to the probability of energy loss per unit length for an electron passing through the environment. The energy loss function occurs in the unauthorized range of electromagnetic waves propagating in a system. One way to stimulate solid electrons is to encourage electrons by other electrons. As a beam of single-energy electrons collides with a solid, electronic energy losses can detect its excitation. Peaks of energy loss are related to optical transmissions and plasmonic oscillations. The most significant peak in the loss spectrum is the peak where $\varepsilon_1(\omega)$ has root and (or is close to its root) and is known as the plasmonic peak, which indicates the mass fluctuations of the electron charge density in the crystal. The maximum peak energies in this spectrum are defined as the energy of the plasmons. Plasmon peaks in the ELoss are located in places where the amplitude of both $\varepsilon_1(\omega)$ and $\varepsilon_2(\omega)$ functions are small. The ELoss curve in part Fig. 5(c) shows that the loss spectrum is very small up to about 20eV, and its characteristic peak occurs at about 20eV, in which one of the roots of the $\varepsilon_1(\omega)$ was also received. This peak represents plasma energy in crystals. Notably, the infrared spectrum in the infrared and visible areas is zero, indicating that the FeVSb compound is a good case for optical applications in these energies.

One of the essential parameters for the design and application of optical devices is the refractive index. The refractive index has a complex function whose relationship is as follows:

$$\tilde{n} = n(\omega) + ik(\omega) \tag{8}$$

In this case, $n(\omega)$ is the real part of the refractive index, where ω is the frequency of the light emitted and $n(\omega) = \frac{c}{v}$,

K is the imaginary part is the refractive index, which is a measure of the amount of electromagnetic radiation absorbed by that substance and named by extinction. The refractive index is a dimensionless measure to determine the decrease in the speed of light or any other beam, and the rate of refraction of radiation in this material. The relationship between the refractive index and the dielectric function is as follows:

$$n(\omega) = \frac{1}{\sqrt{2}}\sqrt{\varepsilon_1(\omega) + \sqrt{(\varepsilon_1(\omega))^2 + (\varepsilon_2(\omega))^2}} \quad (9)$$

According to Fig. 5(d), the static refractive index is 2.5, which shows the semiconductor behavior. As the optical spectrum energy increases, we see a sharp peak at the visible edge, which of course, also indicates optical instability because it suddenly decreases with a very steep slope. Still, the rate of failure has dropped much more than 5 eV.

Another important optical factor is the absorption coefficient, which is calculated according to the following equation:

$$A(\omega) = \frac{2\omega k(\omega)}{c} \quad (10)$$

Due to this relationship, the highest absorption will occur when we have the highest extinction coefficient and the lowest electromagnetic wave passage is given energy. Based on the

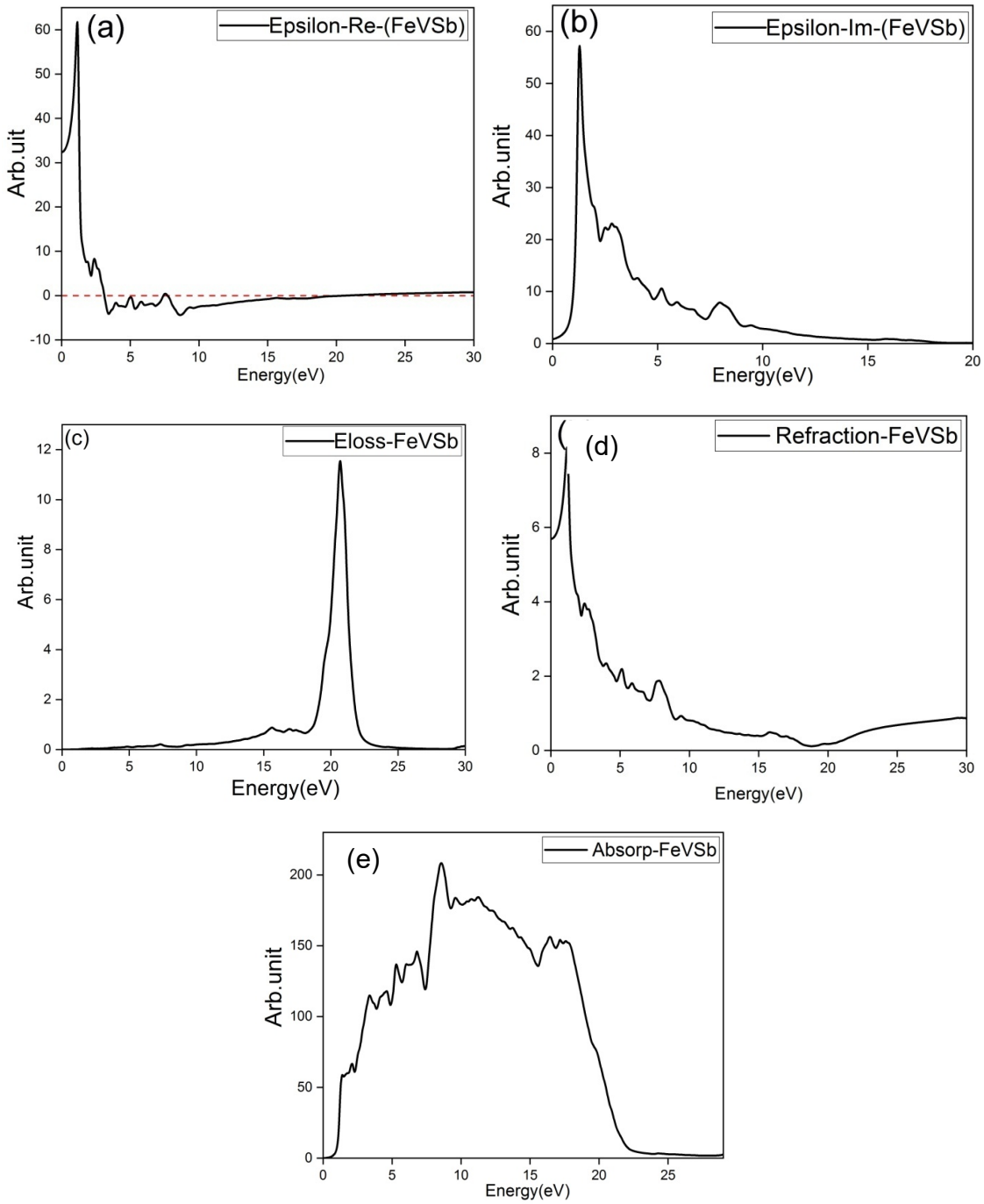

Fig. 5. (a, b) Real and Imaginary parts of dielectric function, (c) ELoss, (d) Refraction, and (e) Absorption indexes of FeVSeb versus photon energy

semiconductor behavior of the FeVSb alloy, it can be seen that no light absorption occurs until about 1 eV. The absorption diagram is still increasing with a very steep slope and has reached its maximum value of about 7 eV. The optical response of this compound has mainly occurred in the infrared and visible regions. On the other hand, the spectrum of the loss function in this optical energy period is very small, so this combination can be considered a suitable candidate for optical and optoelectronic applications in the visible range and the ultraviolet edge.

4. Conclusion

We studied the structural, electronic, and optical properties of the FeVSb compound by applying the computations within the density functional theory framework and using GGA approximation. It was observed that the non-magnetic phase of this compound would be more stable than its ferromagnetic phase. Its lattice constant and the bulk module is obtained following the previous values. Also, the calculation of elastic stability and phonon distribution curves and the phonon density of states clearly show this compound's stability in the half-heusler phase with MgAgAs-type structure. The bandstructure and DOS curve represent the semiconductor behavior with an indirect gap of 0.39 eV in the L-X direction for this combination. The study of optical coefficients and optical response of this compound also indicates good optical absorption in the ultraviolet spectrum and transmission of excited electrons in the visible region. We also see the emergence of super luminescence in energies above the ultraviolet spectrum (from 10 eV onwards) for this compound.

REFERENCES

[1] A. Yamamoto, T. Takeuchi, The Potential of FeVSb half-Heusler phase for practical thermoelectric material, J. Electron. Mater. **46** (5), 3200-3206 (2017).
DOI: https://doi.org/10.1007/s11664-016-4804-y

[2] L. Jodin, J. Tobola, P. Pecheur, H. Scherrer, S. Kaprzyk, Effect of substitutions and defects in half-Heusler FeVSb studied by electron transport measurements and KKR-CPA electronic structure calculations, Phy. Rev. B. **70** (18), 184207 (2004).
DOI: https://doi.org/10.1103/PhysRevB.70.184207

[3] B. Kong, B. Zhu, Y. Cheng, L. Zhang, Q.X. Zeng, X. W. Sun, Structural, mechanical, thermodynamics properties and phase transition of FeVSb, Phys. B: Condens. Matter. **406** (15-16), 3003-3010 (2011). DOI: https://doi.org/10.1016/j.physb.2011.04.067

[4] M. Zou, J.F. Li, P. Guo, T. Kita, Synthesis and thermoelectric properties of fine-grained FeVSb system half-Heusler compound polycrystals with high phase purity, J. Phys. D. **43** (41), 415403 (2010). DOI: https://doi.org/10.1088/0022-3727/43/41/415403

[5] C. Uher, J. Yang, S. Hu, D.T. Morelli, G.P. Meisner, Transport properties of pure and doped MNiSn (M=Zr, Hf), Phys. Rev. B. **59** (13), 8615 (1999).
DOI: https://doi.org/10.1103/PhysRevB.59.8615

[6] S. Sakurada, N. Shutoh, Effect of Ti substitution on the thermoelectric properties of (Zr, Hf) NiSn half-Heusler compounds, Appl. Phys. Lett. **86** (8), 082105 (2005).
DOI: https://doi.org/10.1063/1.1868063

[7] P.G. Van Engen, K.H.J. Buschow, R. Jongebreur, M. Erman, PtMnSb, a material with very high magneto-optical Kerr effect, Appl. Phys. Lett. **42** (2), 202-204 (1983).
DOI: https://doi.org/10.1063/1.93849

[8] F. Casper, H.C. Kandpal, G.H. Fecher, C. Felser, Electronic and magnetic properties of GdPdSb, J. Phys. D. **40** (10), 3024 (2007).
DOI: https://doi.org/10.1088/0022-3727/40/10/002

[9] S.Y. Lin, M. Chen, X.B. Yang, Y.J. Zhao, S.C. Wu, C. Felser, B. Yan, Theoretical search for half-Heusler topological insulators, Phys. Rev. B. **91** (9), 094107 (2015).
DOI: https://doi.org/10.1103/PhysRevB.91.094107

[10] X. Zhang, et al. NMR evidence for the topologically nontrivial nature in a family of half-Heusler compounds, Sci. Rep. **6**, 23172 (2016). DOI: https://doi.org/10.1038/srep23172

[11] R. Pöttgen, D. Johrendt, Equiatomic intermetallic europium compounds: syntheses, crystal chemistry, chemical bonding, and physical properties, Chem. Mater. **12** (4), 875-897 (2000).
DOI: https://doi.org/10.1021/cm991183v

[12] S. Gupta, K.G. Suresh, Review on magnetic and related properties of RTX compounds, J. Alloys Compd. **618**, 562-606 (2015).
DOI: https://doi.org/10.1016/j.jallcom.2014.08.079

[13] C. Fu, H. Xie, Y. Liu, T.J. Zhu, J. Xie, X.B. Zhao, Thermoelectric properties of FeVSb half-Heusler compounds by levitation melting and spark plasma sintering, Intermetallics **32**, 39-43 (2013).
DOI: https://doi.org/10.1016/j.intermet.2012.07.037

[14] R. Hasan, S.C. Ur, Synthesis of FeVSb 1− x Se x Half-Heusler Alloys via Mechanical Alloying and Evaluation of Transport and Thermoelectric Properties, J. Electron. Mater. **49**, 2719-2725 (2020). DOI: https://doi.org/10.1007/s11664-019-07653-1

[15] A. El-Khouly, A. Novitskii, A.M. Adam, A. Sedegov, A. Kalugina, D. Pankratova, D. Karpenkov, V. Khovaylo, Transport and thermoelectric properties of Hf-doped FeVSb half-Heusler alloys, **820**, 153413 (2020).
DOI: https://doi.org/10.1016/j.jallcom.2019.153413

[16] J. Yang, H. Li, T. Wu, W. Zhang, L. Chen, J. Yang, Evaluation of half-Heusler compounds as thermoelectric materials based on the calculated electrical transport properties, Adv. Funct. Mater. **18** (19), 2880-2888 (2008).
DOI: https://doi.org/10.1002/adfm.200701369

[17] D.P. Young, P. Khalifah, R.J. Cava, A.P. Ramirez, Thermoelectric properties of pure and doped FeMSb (M= V, Nb), J. Appl. Phys. **87** (1), 317-321 (2000). DOI: https://doi.org/10.1063/1.371863

[18] Y. Stadnyk, et al., Crystal structure, electrical transport properties and electronic structure of the VFe1− xCuxSb solid solution, J. Alloys Compd. **402** (1-2), 30-35 (2005).
DOI: https://doi.org/10.1016/j.jallcom.2005.04.186

[19] A. El-Khouly, et al., Transport and thermoelectric properties of Hf-doped FeVSb half-Heusler alloys, J. Alloys Compd. **820**, 153413 (2020).

[20] Ş. Ţălu, et al., Microstructure and Tribological Properties of FeNPs@a-C:H Films by Micromorphology Analysis and Frac-

tal Geometry, Ind. Eng. Chem. Res. **54** (33), 8212-8218 (2015). DOI: https://doi.org/10.1021/acs.iecr.5b02449

[21] M. Zare, et al., Evolution of rough-surface geometry and crystalline structures of aligned TiO_2 nanotubes for photoelectrochemical water splitting, Scientific Reports **8**, 10870 (2018). DOI: https://doi.org/10.1038/s41598-018-29247-3

[22] A. Boochani, et al., Novel Graphene-like Co_2VAl (111): Case Study on Magnetoelectronic and Optical Properties by First-Principles Calculations, J. Phys. Chem. C. **121** (7), 3978-3986 (2017). DOI: https://doi.org/10.1021/acs.jpcc.6b10572

[23] A. Achour, M. Islam, S. Solaymani, S. Vizireanu, K. Saeed, G. Dinescu, Influence of plasma functionalization treatment and gold nanoparticles on surface chemistry and wettability of reactive-sputtered TiO_2 thin films, Appl. Surf. Sci. **458**, 678-685 (2018). DOI: https://doi.org/10.1016/j.apsusc.2018.07.145

[24] K. Schwarz, P. Blaha, G.K.H. Madsen, Electronic structure calculations of solids using the WIEN2k package for material sciences, Comput. Phys. Commun. **147** (1-2), 71-76 (2002). DOI: https://doi.org/10.1016/S0010-4655(02)00206-0

[25] J.P. Perdew, et al., Restoring the density-gradient expansion for exchange in solids and surfaces, Phys. Rev. Lett. **100** (13), 136406 (2008). DOI: https://doi.org/10.1103/PhysRevLett.100.136406

[26] D. Alfè, PHON: A program to calculate phonons using the small displacement method, Comput. Phys. Commun. **180** (12), 2622-2633 (2009). DOI: https://doi.org/10.1016/j.cpc.2009.03.010

[27] S.R. Maalouf, S.S.Vel, Nonlinear elastic analysis of 2D materials of arbitrary symmetries with application to black phosphorus, Mech. Mater. **165**, 104159 (2022). DOI: https://doi.org/10.1016/j.mechmat.2021.104159

[28] T. Fang, X. Zhao, T. Zhu, Band structures and transport properties of high-performance Half-Heusler thermoelectric materials by first principles, Materials **11** (5), 847 (2018). https://doi.org/10.3390/ma11050847

[29] G.S. Neumann, L. Stixrude, R E. Cohen, First-principles elastic constants for the hcp transition metals Fe, Co, and Re at high pressure, Phys. Rev. B **69**, 219903 (2004). DOI: https://doi.org/10.1103/PhysRevB.69.219903

[30] S.F. Pugh, XCII. Relations between the elastic moduli and the plastic properties of polycrystalline pure metals, Lond. Edinb. Dublin Philos. Mag. J. Sci. **45** (367), 823-843 (1954). DOI: https://doi.org/10.1080/14786440808520496

[31] Y. Tian, B. Xu, Z. Zhao, Microscopic theory of hardness and design of novel superhard crystals, IJRMHM. **33**, 93-106 (2012). DOI: https://doi.org/10.1016/j.ijrmhm.2012.02.021

[32] M.E. Fine, L.D. Brown, H.L. Marcus, Elastic constants versus melting temperature in metals, Scripta Metallurgica **18** (9), 951-956 (1984). DOI: https://doi.org/10.1016/0036-9748(84)90267-9

[33] Z.Q. Lv, Z.F. Zhang, Q. Zhang, Z.H. Wang, S.H. Sun, W.T. Fu, Structural, electronic and elastic properties of the Laves phases WFe2, MoFe2, WCr2 and MoCr2 from first-principles, Solid State Sci. **56**, 16-22 (2016). DOI: https://doi.org/10.1016/j.solidstatesciences.2016.03.012

[34] H. Shi, W. Ming, D.S. Parker, M.H. Du, D.J. Singh, Prospective high thermoelectric performance of the heavily p-doped half-Heusler compound CoVSn, Phys. Rev. B, **95** (19), 195207 (2017). DOI: https://doi.org/10.1103/PhysRevB.95.195207

[35] Y. Wang, J. Cheng, M. Behtash, W. Tang, J. Luo, K. Yang, First-principles studies of polar perovskite KTaO 3 surfaces: structural reconstruction, charge compensation, and stability diagram, Phys. Chem. Chem. Phys. **20** (27), 18515-18527 (2018). DOI: https://doi.org/10.1039/C8CP02540A

[36] Y. Jiang, Y. Shi, X. Xiang, J. Qi, Y. Han, Z. Liao, T. Lu, Thermodynamic Stabilities of Perfect and Vacancy-Defected Li 2 Ti O 3 (001) Surfaces From First-Principles Analyses, Phys. Rev. App. **11** (5), 054088 (2019). DOI: https://doi.org/10.1103/PhysRevApplied.11.054088